be reported in part II, this primary ordering is well established, even in samples quenched rapidly from the melt. The ordering of the thorium atoms within the $(001)_p$ 'half-occupied' planes is, however, of a very short-range nature. The corresponding diffraction effects are very diffuse and their rod-like nature indicates a lack of long-range correlations *between* $\{110\}_p$ *planes* of thorium atoms. The average correlation length is only 20–30 Å.

Within the $\{110\}_p$ planes the *average* ordering periodicities are maintained over distances of the order of hundreds of ångströms. However, presumably due to the difficulty of diffusion of the large, highly charged thorium cations, only an average long-period ordering is observed, which is adequately described by a sinusoidal modulation.

Accompanying the thorium/vacancy density modulation, there is a modulation of atom displacements. The niobium displacements shown in Fig. 6 have been quite accurately established from the structure refinement. In general there is a displacement of all niobium atoms *away* from the occupied thorium sites towards the empty channels, *i.e.* there is an attempt by the niobium cations to balance the highly anisotropic charge distribution formed by the clustering of the tetravalent thorium cations into columns. The displacements are maximum for the niobiums which are associated with the highest density of thoriums (see Fig. 6), *i.e.* the amplitudes of the niobium displacements follow the same modulation pattern as the thorium density modulation. The maximum niobium displacements are about 0·25 Å, which are considerably larger than those observed in perovskites such as $NaNbO_3$ and $KNbO_3$ (Megaw, 1968).

Finally, in the ordering hierarchy, we have an ordered series of oxygen displacements which corresponds to a tilting of the octahedral framework about $\langle 110\rangle_p$ axes, parallel to the columns of thorium atoms. The angle of tilt is about 8°, individual oxygen displacements are in the range 0·2–0·5 Å. The tilts are accompanied by displacements of thorium atoms perpendicular to the $[1\bar{1}0]_p$ columns, see Table 1.

The hierarchy of ordering patterns and the associated correlation lengths are directly related to the formation of microdomains, with domain boundaries parallel to $(100)_p$ and $(010)_p$ and average widths of 25 Å. The description of the microdomain model for $ThNb_4O_{12}$ will be given in a subsequent publication (part II).

We thank the Instituto de Química Inorgánica 'ELHUYAR', CSIC, Spain, for allowing us to use their electron microscopy facilities.

References

BURBANK, R. D. (1970). *J. Appl. Cryst.* **3**, 112–120.
GLAZER, A. M. (1972). *Acta Cryst.* B**28**, 3384–3392.
KELLER, C. (1965). *J. Inorg. Nucl. Chem.* **27**, 1233–1246.
KOVBA, L. M. & TRUNOV, V. K. (1962). *Dokl. Akad. Nauk SSSR*, **147**, 622–624.
LABEAU, M. & JOUBERT, J. C. (1978). *J. Solid State Chem.* **25**, 347–353.
MEGAW, H. D. (1968). *Acta Cryst.* A**24**, 589.
OGAWA, S. (1962). *J. Phys. Soc. Jpn*, **17**, Suppl. BII, 253–262.
TRUNOV, V. K. & KOVBA, L. M. (1966). *Zh. Strukt. Khim.* **7**, 896–897.

Acta Cryst. (1982). A**38**, 186–194

α-Bungarotoxin Structure Revealed by a Rapid Method for Averaging Electron Density of Non-crystallographically Translationally Related Molecules

BY DAVID A. AGARD AND ROBERT M. STROUD*

University of California at San Francisco, Department of Biochemistry and Biophysics, School of Medicine, San Francisco, California 94143, *USA*

(*Received* 7 *November* 1980; *accepted* 11 *June* 1981)

Abstract

In macromolecular crystallography multiple and independent images of the same chemical species are often present in the crystallographic asymmetric unit. Averaging of density for non-crystallographically related molecules is a powerful technique both for improvement of the density image, and for subsequent phase refinement. Surprisingly often, a non-crystallographic axis of symmetry lies parallel to a crystallographic axis. In such cases, the averaged electron density map can be computed simply and directly from

* To whom reprint requests should be sent.

0567-7394/82/020186-09$01.00

the observed structure factors without subsequent interpolation or averaging in the molecular density map. The procedure described is much more efficient than averaging with consequent interpolation in the real-space domain. The same algorithm can be used in reverse both for very rapid computation of the Fourier transform $F_c(\mathbf{s})$ of a unit cell based on replacement of the 'averaged' density image for the non-crystallographically related molecules, and consequently for a rapid translation function search based on minimization of $R = \sum ||F_o| - |F_c||/\sum |F_o|$ directly. This residual is much more sensitive than any 'Patterson' search technique where there is overlap between inter- and intramolecular vectors. Jointly these rapid analytic techniques for density averaging and subsequent computation of calculated structure factors from the averaged density map were used to solve and refine the crystal structure of α-bungarotoxin. The rapid translation search and averaging procedures were crucial to the solution of the α-bungarotoxin structure which is described.

Introduction

Many examples now exist where macromolecules crystallize with more than one molecule per crystallographic asymmetric unit (as.u.); the most striking instance perhaps being the regular icosahedral or helical viruses (Harrison, Olson, Schutt, Winkler & Bricogne, 1978; Bloomer, Champness, Bricogne, Staden & Klug, 1978). If all of the molecules in the as.u. are identical, the resultant non-crystallographic symmetry (NCS) implies a powerful joint relationship amongst the phases. Both Rossmann and co-workers (Rossmann & Blow, 1963; Main & Rossmann, 1966) and Bricogne (1974, 1976) have developed formalisms for utilizing the real-space redundancy to constrain or refine experimentally derived phases. Bricogne's approach has proven to be the most useful for macromolecular structural problems. The principle behind both methods derives from the fact that inaccuracies in the experimentally determined, or even refined, phase terms will cause the electron density calculated for the NCS-related molecules to be non-equivalent. An improved estimation of the 'true' molecular density distribution can be obtained by averaging the related density for NCS-related molecules. A new set of phases can then be derived by back-transforming the density map with 'averaged' density images for the NCS molecules. The improved phases are associated with observed amplitudes and a new density map computed. The entire process is reiterated until convergence is reached, generating an improved set of phases consistent with the constraints implied by non-crystallographic symmetry. The coherent identical components of the density are reinforced while incoherent or non-identical noise components are diminished at each cycle. For a detailed description of this approach, see Bricogne (1974, 1976).

A linear analysis of the phase constraints implied by the presence of non-crystallographic symmetry has been presented by Crowther (1967, 1969). More recently Jack (1973) provided equations for the special case of pure rotational NCS for phasing the centric projection of tobacco mosaic virus. In those cases where the rotational part of the NCS is parallel to a crystallographic axis and a subset of the Laue symmetry about that axis (*e.g.* a twofold NCS rotation in the cell of space group $P2_12_12_1$ as in bungarotoxin) the NCS can be considered as arising from pure translationally related molecules. Where all or part of the NCS can be considered as purely translational [*e.g.* in crystals of α-bungarotoxin (Spencer, 1977; Agard, Spencer & Stroud, 1981), lac repressor core (Steitz, 1980), glutamine synthetase (Heidner *et al.*, 1978) and melitin (Eisenberg, 1980)], a more efficient approach to molecular averaging than the real-space method suggested by Bricogne (1974) can be utilized. Described here, along with application to the low-resolution structure determination of the snake neurotoxin α-bungarotoxin, is a technique where the averaging is performed as a simple multiplication in reciprocal space. Although the equations derived here represent a subset of those developed by Rossmann & Blow (1963, 1964), Main & Rossmann (1966) and Crowther (1967), the great simplification afforded by pure translational NCS justifies their presentation. For pure translations of the kind described above no interpolations are required with this approach, so providing significant increases in speed and accuracy over conventional methods.

Theory of the method

(i) *The translation operation*

Let $\rho_m(\mathbf{r})$ represent the electron density distribution of one molecule and $F_m(\mathbf{s})$ be its Fourier transform as defined by

$$F_m(\mathbf{s}) = \int_{V_m} \rho_m(\mathbf{r}) \exp[2\pi i(\mathbf{r}.\mathbf{s})]\, d\mathbf{r}, \qquad (1)$$

where V_m is the volume containing the density for the molecule m, and $\mathbf{r}$, $\mathbf{s}$ represent real- and reciprocal-space vectors respectively. Translation of $\rho_m(\mathbf{r})$ by a vector Δ causes the phase of $F_m(\mathbf{s})$ to be shifted by $2\pi\Delta.\mathbf{s}$ while leaving the amplitude unchanged:

$$F'_m(\mathbf{s}) = \int_{V_m} \rho_m(\mathbf{r}) \exp[2\pi i(\mathbf{r} + \Delta).\mathbf{s}]\, d\mathbf{r}$$

$$F'_m(\mathbf{s}) = F_m(\mathbf{s}) \exp[2\pi i(\Delta.\mathbf{s})]. \qquad (2)$$

The Fourier transform of a collection of N equivalent molecules related by N translations Δ_j for $j = 1 - N$

can be described in terms of the Fourier transform of a single molecule $F_m(\mathbf{s})$ by expansion of (2).

$$F(\mathbf{s}) = F_m(\mathbf{s}) \sum_{j=1}^{N} \exp[2\pi i(\boldsymbol{\Delta}_j . \mathbf{s})]$$
$$F(\mathbf{s}) = F_m(\mathbf{s})\, F_t(\mathbf{s}) \qquad (3)$$

where now

$$F_t(\mathbf{s}) = \sum_{j=1}^{N} \exp[2\pi i(\boldsymbol{\Delta}_j . \mathbf{s})].$$

$F_t(\mathbf{s})$ is independent of the molecular transform and arises solely from the non-crystallographic symmetry.

From another viewpoint, the reciprocal-space multiplication implied by (3) is equivalent to a real-space convolution of ρ_m with N delta functions appropriately located in the unit cell (*i.e.* at the positions $\boldsymbol{\Delta}_j$ for $j = 1 - N$). This equivalence is exploited in the averaging method.

(ii) *Density averaging*

If an observed set of amplitudes $|F_o(\mathbf{s})|$ and phases $\varphi(\mathbf{s})$ have been obtained, the electron density for the unit cell is given by

$$\rho_0(\mathbf{r}) = \frac{1}{V} \sum_{s} F_o(\mathbf{s}) \exp(-2\pi i\, \mathbf{r} . \mathbf{s}),$$

where (4)

$$F_o(\mathbf{s}) = |F_o(\mathbf{s})| \exp[i\varphi(\mathbf{s})].$$

This map will contain N different images of the molecule at positions $\boldsymbol{\Delta}_j$. It is convenient to set $\boldsymbol{\Delta}_1 = 0$, so fixing the origin: *i.e.* $\rho_m(\mathbf{r})_{(j=1)}$ corresponds to the density for the first molecule with respect to the unit-cell origin at $\mathbf{r} = 0$. Translation of the entire unit-cell density map by $-\boldsymbol{\Delta}_j$ leads to superposition of the experimentally determined images for the jth and first molecules. Thus, the Fourier transform of

$$F_o(\mathbf{s})[1 + \exp(-2\pi i \boldsymbol{\Delta}_j . \mathbf{s})] \qquad (5)$$

will superimpose and add density for the jth and first molecules at the position of the first molecule. Outside of the molecular volume V_m the superposition will be of non-equivalent (non-NCS related) parts of the unit cell, and will be meaningless. All NCS molecules may be summed, and averaged by:

$$\bar{\rho}_0(\mathbf{r}) = \frac{1}{NV} \sum F_o(\mathbf{s}) \left[\sum_{j=1}^{N} \exp(-2\pi i \boldsymbol{\Delta}_j . \mathbf{s}) \right] \times \exp(-2\pi i\, \mathbf{r} . \mathbf{s}) \qquad (6)$$

where $\boldsymbol{\Delta}_1 = 0$.

Thus, $\bar{\rho}_0(\mathbf{r})$ is given directly as the Fourier transform of the modified coefficients

$$F_o(\mathbf{s}) \left[\sum_{j=1}^{N} \exp(-2\pi i \boldsymbol{\Delta}_j . \mathbf{s}) \right]. \qquad (7)$$

$\bar{\rho}_0(\mathbf{r})$ now contains the averaged density for all NCS-related molecules, with incoherent overlap contributing to other regions of the map everywhere else. It must be emphasized that this procedure does not depend on knowing anything about V_m, the volume shape of each molecule. Indeed, the $\bar{\rho}_0(\mathbf{r})$ maps will be the means of best defining V_m. The $\boldsymbol{\Delta}_j$ are readily obtained from the Patterson map for the native protein structure and if necessary can be refined later using the rapid translation/R-factor search described below.

Since the averaged map $\bar{\rho}_0(\mathbf{r})$ (equation 6) will contain only one copy of the averaged molecule, it will always be of triclinic ($P1$) symmetry, no matter what the space group of the crystals is. Correspondingly, the modified $F(\mathbf{s})$ produced in (3) must be calculated for all h, k, and for $l > 0$. This increase in the number of input $F(\mathbf{s})$ to a triclinic ($P1$) fast Fourier transform is compensated for by the fact that it is only necessary to compute $\bar{\rho}_0(\mathbf{r})$ over the volume of a single molecule. Because the averaging is performed in reciprocal space the translations are analytically incorporated; hence, no interpolations are required. The result is a dramatic increase in the speed and accuracy over a conventional approach (*e.g.* involving averaging by interpolation in the real-space domain). Only the first molecule, over which all others have been placed, will be properly averaged, the remainder of the density map outside V_m will be completely scrambled. This is a direct consequence of translating the entire unit cell by the local translational symmetry between molecules.

Since the averaging process does not require the definition of a molecular boundary, solvent regions immediately surrounding the molecule, if they are represented around each molecule, are correctly averaged. Iterative phase refinement, however, does require that the molecular envelope be defined, a task simplified with the averaged density map.

(iii) *Crystallographic symmetry and calculation of* $F_c(\mathbf{s})$

For efficiency in the total NCS refinement procedure, and for application of the molecular density transform to rapid translation search, it is necessary to build the calculated structure factor $F_c(\mathbf{s})$ for the entire unit cell directly from the transform of one averaged molecular image,

$$F_m(\mathbf{s}) = \int_{V_m} \bar{\rho}_0(\mathbf{r}) \exp(2\pi i\, \mathbf{r} . \mathbf{s})\, d\mathbf{r}. \qquad (8)$$

The contributions from shifted and symmetry-related molecules are added vectorally to $F_c(\mathbf{s})$ as follows. The coordinate transformation corresponding to the ith crystallographic symmetry element is described by a

rotation matrix A_i and a translation vector $\mathbf{t}_i$, for M molecules related by crystallographic symmetry. Thus, by analogy with (3), $F''_m(\mathbf{s})$ – the transform of crystallographic symmetry-related and translated molecules – becomes

$$F''_m(\mathbf{s}) = \sum_{i=1}^{M} F_m(A_i^T\,\mathbf{s}) \exp(2\pi i\,\mathbf{t}_i.\,\mathbf{s}), \qquad (9)$$

where A^T is the transpose of matrix A.

Finally, including N_j non-crystallographic translations (Δ_j) which apply among each of the M crystallographically related sets of molecules, the transform of the whole unit cell $F_c(\mathbf{s})$ becomes

$$F_c(\mathbf{s}) = \sum_{i=1}^{M} F_m(A_i^T\,\mathbf{s}) \sum_{j=1}^{N} \exp\{2\pi i[(A_i\,\Delta_j + \mathbf{t}_i).\,\mathbf{s}]\}$$

or

$$F_c(\mathbf{s}) = \sum_{i=1}^{M} F_{m_i}(\mathbf{s})\,F_{t_i}(\mathbf{s}), \qquad (10)$$

where now

$$F_{m_i}(\mathbf{s}) = F_m(A_i^T\,\mathbf{s})$$

and

$$F_{t_i}(\mathbf{s}) = \sum_{j=1}^{N} \exp\{2\pi i[(A_i\,\Delta_j + \mathbf{t}_i).\,\mathbf{s}]\}. \qquad (11)$$

$F_{t_i}(\mathbf{s})$ is easily calculated, and for crystallographic rotations the values $F_{m_i}(\mathbf{s})$ are already contained in $F_m(\mathbf{s})$ [*i.e.* $F_m(A_i^T\,\mathbf{s})$] computed in (8).

(iv) *Optimum translation search*

The separation of terms F_m and F_t in (10) provides great simplification in the calculation of $F_c(\mathbf{s})$ from the density for a single image, and provides the basis for a rapid translation search where changes in Δ_j of F_t are assayed directly in the conventional crystallographic residual. This procedure was crucial to the solution of both α-bungarotoxin and cobrotoxin in our laboratory.

The translation function search was developed independently from that described by Nixon & North (1976), although it is of similar form. The values of Δ_j can be refined to minimize the residual

$$R = \sum ||F_o(\mathbf{s})| - |F_c(\mathbf{s})||/\sum |F_o(\mathbf{s})| \qquad (12)$$

by the simple computation of $F_{t_i}(\mathbf{s})$ [$F_{m_i}(\mathbf{s})$ is only calculated once] for all Δ_j. This 'reciprocal-space' translation function has a much higher signal-to-noise ratio than Patterson search techniques since it searches only for *inter*molecular vectors, where a Patterson search implies a search for intermolecular vectors in a map which includes both inter- and intramolecular vectors.

(v) *Density map refinement*

The separation of terms in (6), (7) and (10), (11) permits density map refinement without any interpolation. Rapid density averaging (equations 6, 7) leads to the initial averaged map. $\bar{\rho}_m(\mathbf{s})$ is extracted from $\bar{\rho}_0(\mathbf{r})$ by multiplication with a boundary function $g(\mathbf{r})$ that has values of unity inside V_m and zero outside. Next, this average density for a single molecule is Fourier transformed to yield $F_m(\mathbf{s})$ (equation 8) which is used in (10) to reconstruct the structure factors of the unit cell. Lastly, the phases of $F_c(\mathbf{s})$ are associated with the observed $|F_o(\mathbf{s})|$ (with a weighting scheme if desired), and Fourier transformed to provide a new electron density map. These operations can be re-iterated until no further improvement in the electron density map is observable. Since no interpolations are required, substantial improvements in accuracy and computation time can be achieved.

Application to α-bungarotoxin

α-Bungarotoxin is a polypeptide α-neurotoxin of molecular weight 8000 daltons isolated from the venom of the banded krait *Bungarus multicinctus* (Chang & Lee, 1963). Two orthorhombic crystal forms have been obtained by Spencer and Stroud (Spencer, 1977), a 'large-cell' form ($a = 69{\cdot}9$, $b = 76{\cdot}7$, $c = 44{\cdot}8$ Å) with

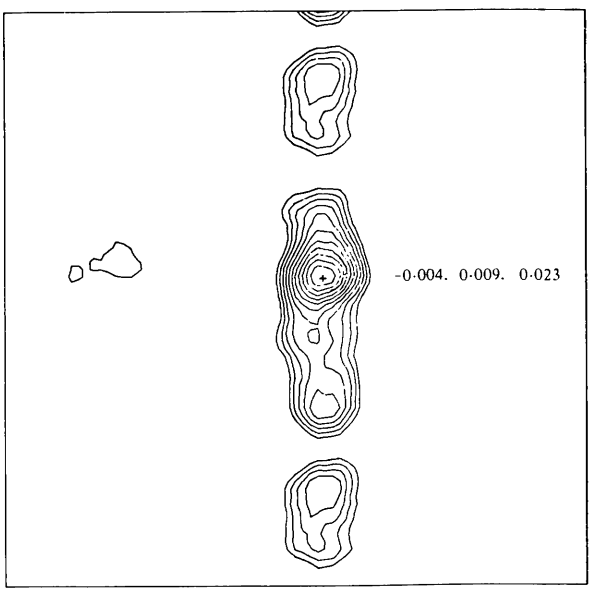

Fig. 1. A section through the translation function relating the electron density from the averaged half cell to the small-cell form ($x = -0{\cdot}12$–$0{\cdot}12$, $y = 0{\cdot}008$, $z = -0{\cdot}35$–$0{\cdot}35$; x horizontal, z vertical). The peak corresponding to a crystallographic residual of about 40% indicates a fractional translation of (−0·004, 0·008, 0·023). Contour levels are at 1% intervals; the function $1 - R$ is plotted to show the correct location as a peak.

four molecules per asymmetric unit and a 'small-cell' form [a' ($\simeq a$) = 67·8, b' ($\simeq b$) = 78·4, c' ($\simeq c/2$) = 22·4 Å] with two molecules per asymmetric unit.

The native Patterson function for the large-cell form shows that four molecules within the asymmetric unit are related by pure translational non-crystallographic symmetry. The small-cell form obtained under slightly different conditions has almost identical a and b cell dimensions, and half-size c dimension. Thus, the native Patterson for the small-cell form and the NCS vectors show that packing in the small-cell form is almost identical to that in the large-cell form. The large cell consists of two almost equivalent halves in the c direction, which become truly equivalent in the small-cell form. The NCS translational vector between pairs of molecules in the small cell is (uvw) = 0·416**a** − 0·341**b** + 0·5**c**. [The additional pure-translational NCS vector in the *large* cell is parallel to the c axis, (uvw) = 0·53**c**.]

The structure was solved initially to 5 Å resolution for the averaged half cell, in the large-cell form, by multiple isomorphous replacement methods [Spencer and Stroud (Spencer, 1977)]. The assumption of equivalence between the two halves becomes invalid beyond about 5 Å resolution. Since this assumption is required to achieve the solution, analysis of this form is restricted to 5 Å resolution. To circumvent this problem, attention was turned to the small-cell form: this was solved by placement – and refinement – of the 'averaged' density map obtained from the large-cell form.

The final 5 Å averaged density map for the large-cell form was calculated with (6). The correct placement of molecules for the small-cell form was obtained with this 5 Å MIR *density map*, instead of an atomic model *via* the translational search (equations 10, 11, 12). A section through the translation function showing the correct location of the large-cell electron density in the small cell (−0·004, 0·008, 0·023; R = 40%) is shown in Fig. 1. The background in this map is R = 55 ± 0·8%. The minimum was the lowest trough in the entire map, about 19σ below the background level. This indicates that α-bungarotoxin molecules undergo a systematic rearrangement on conversion from the large-cell form to the small-cell form. Accurate determination of these shifts in molecular packing is a crucial 'first step' in the phase refinement procedure.

These initial phases for the small-cell form were refined by three cycles of non-crystallographic averaging and phase refinement. The final phases differed from initial phases by 67° on average, and were essentially the same at all resolutions. The net result was a much improved 5 Å resolution density map computed from the small-cell data. The calculated data were compared to the observed $|F_o(\mathbf{s})|$ with the standard crystallographic residual (equation 12) which dropped from 40 to 30%. The final averaged 5 Å density map is shown in Fig. 2.

In an effort to extend the structural analysis to higher resolution, MIR phases were calculated for the averaged half-cell in the large-cell form to 4 Å. Since the assumption of equivalence between the two halves in the large-cell form is invalid beyond 5 Å, these calculated phases were greatly in error. From the positions and molecular boundary defined by the 5 Å analysis, the 4 Å phases were transferred to the small-cell form. The electron density map calculated with these phases and the small-cell $|F_o|$ (Fig. 3)

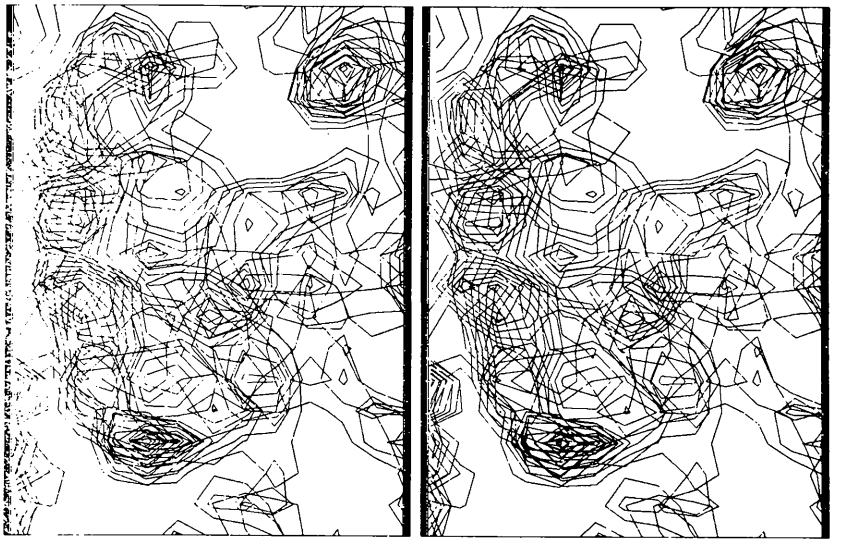

Fig. 2. A region through the final averaged 5 Å small-cell maps shown in stereo (x = 0·23–0·73, y = 0·38–0·69, z = 0·8–1·3; x horizontal, y vertical).

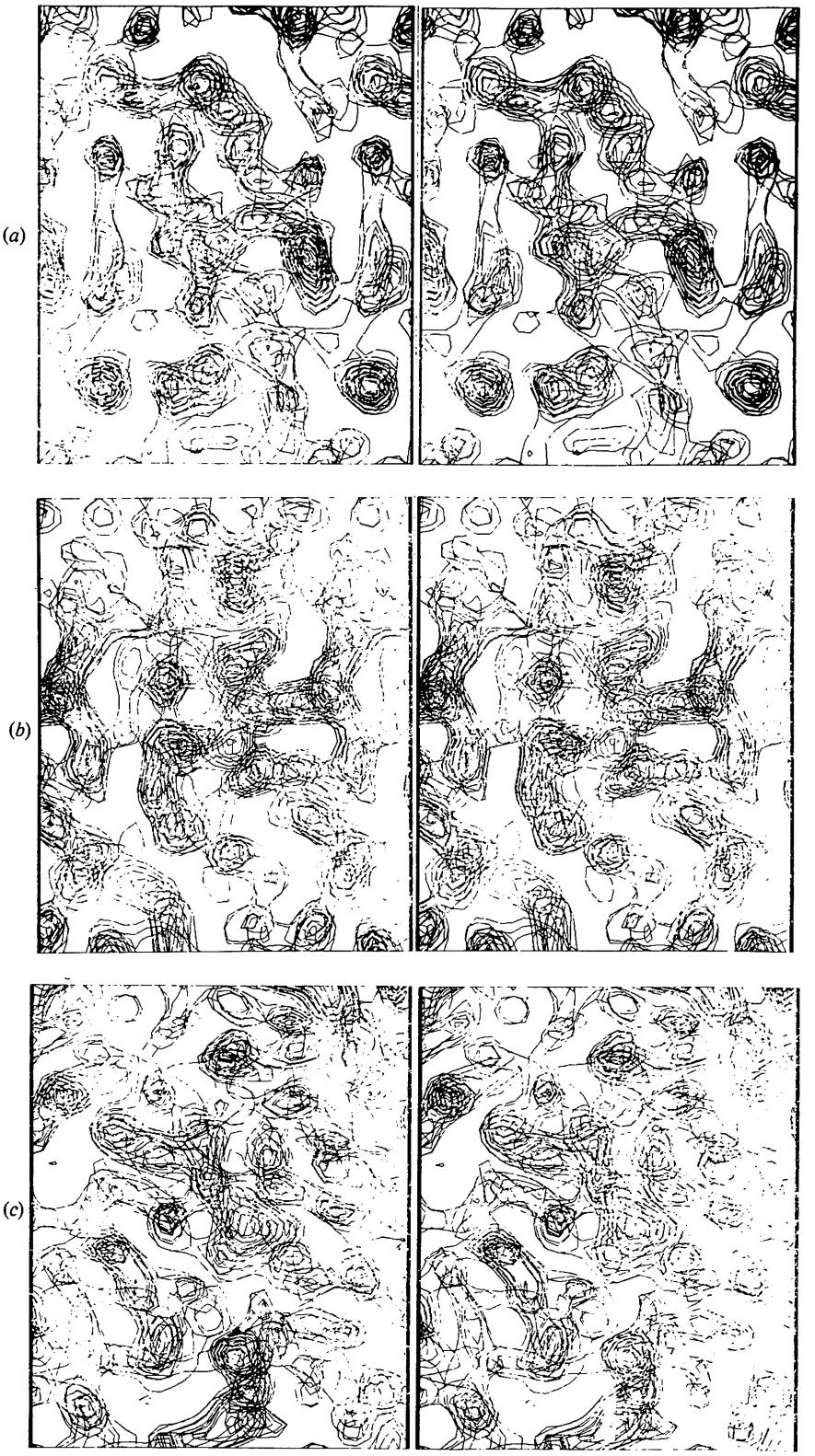

Fig. 3. Stereo plots of three different regions through the starting 4 Å map in the small cell. (*a*) $x = 0{\cdot}18$–$0{\cdot}75$, $y = 0{\cdot}53$–$0{\cdot}6$; (*b*) $x = 0{\cdot}18$–$0{\cdot}75$, $y = 0{\cdot}59$–$0{\cdot}67$, $z = 0$–$1{\cdot}4$, sectioned down y, z horizontal; (*c*) $x = 0{\cdot}23$–$0{\cdot}7$, $y = 0{\cdot}3$–$0{\cdot}8$, $z = 0{\cdot}3$–$0{\cdot}6$, sectioned down z, x horizontal.

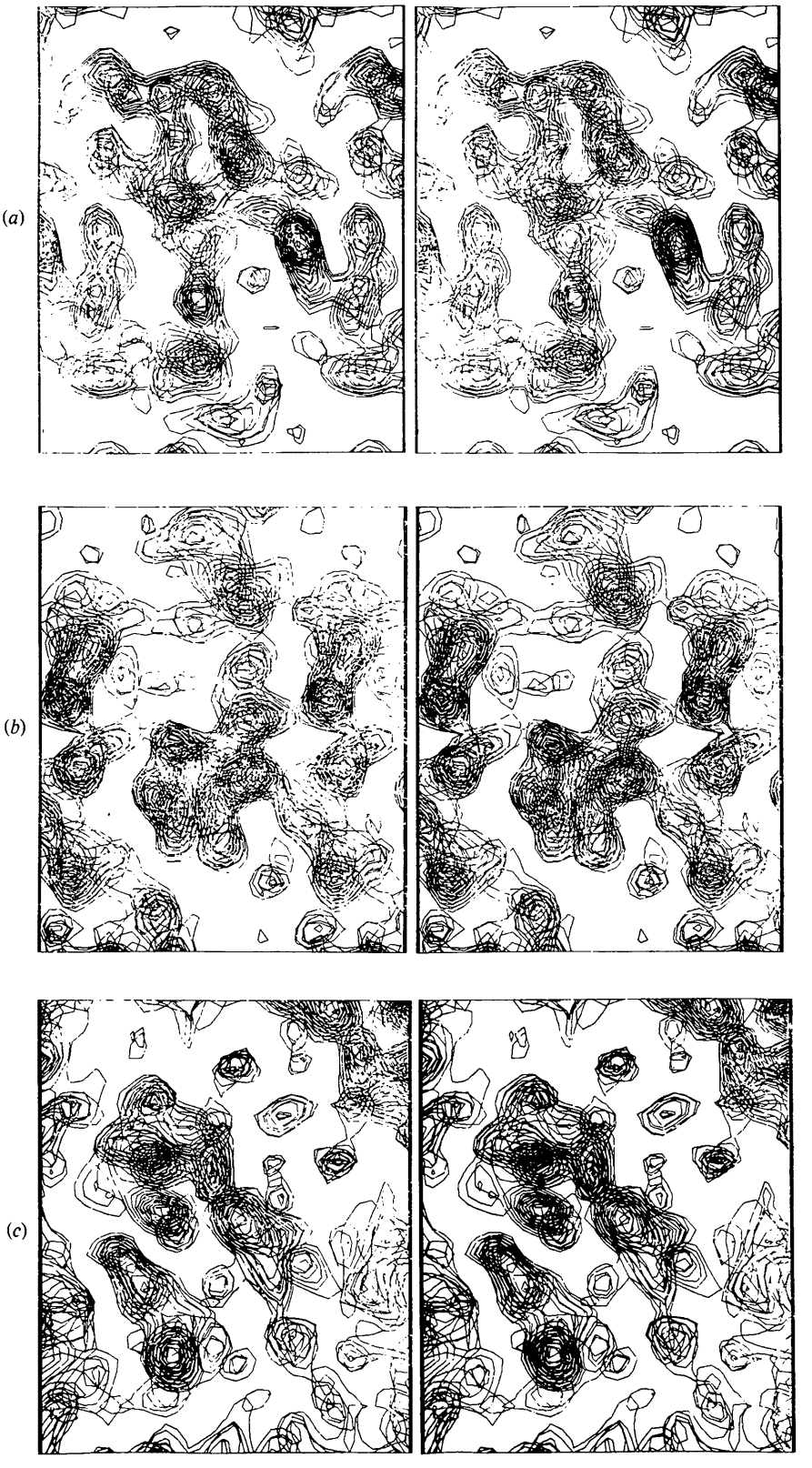

Fig. 4. Stereo plots of the same three regions shown in Fig. 3 but after the non-crystallographic symmetry averaging/phase refinement process was completed.

became the starting point for three cycles of non-crystallographic phase averaging with the procedures described above. Throughout the refinement process, new averaged electron density maps were computed with Sim's (1959) weighted $2|F_o| - |F_c|$ amplitudes.

The correct molecular boundary was redefined and three more cycles of density map refinement reduced the residual from 35 to 20% and gave the much improved map shown in Fig. 4. The overall r.m.s. change in phase between final phases and MIR phases was 69° between 10 and 4 Å resolution (72° between 5 and 4 Å resolution).

The main-chain connectivity was unambiguously established from this map as well as the location of the five disulphide cross bridges and many of the larger side chains. A Lab-Quip molecular model was built to the map with an optical comparator (Richards, 1968). Subsequently, 3·5 Å data was included and the structure was refined by the difference Fourier method (Chambers & Stroud, 1977, 1979) to a residual of 23%. NCS-related molecules were treated as identical throughout. A final $F_o - F_c$ difference map indicated that there was no systematic difference between the two NCS-related molecules. A section through the 3·5 Å averaged $2F_o - F_c$ map is shown in Fig. 5(*a*). The α-carbon structure is presented in Fig. 5(*b*).

Discussion

The power of the procedure described above is emphasized by the fact that the structure analysis of bungarotoxin has withstood attack by conventional MIR methods, by use of Patterson search (rotation

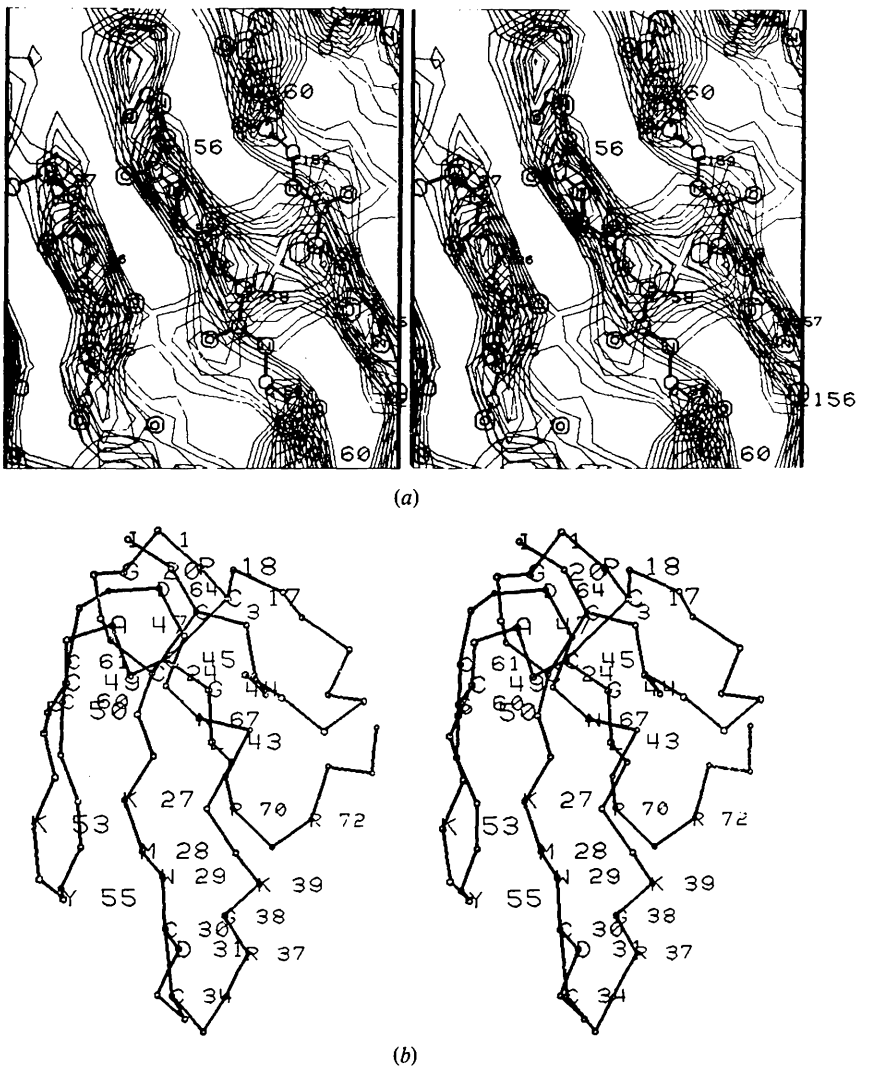

Fig. 5. (*a*) A stereo plot of a region of the final $2F_o - F_c$ 3·5 Å map showing the non-crystallographic diad axis. Three strands of the four-stranded anti-parallel β-structure spanning the intermolecular interface are also shown. (*b*) The complete α-carbon diagram in stereo.

function) analysis with the structure of erabutoxin (Tsernoglou & Petsko, 1976; Low *et al.*, 1976), which in hindsight is not surprising in view of the unexpectedly large differences in folding of the two molecules, and by all attempts to interpret the 5 Å MIR map (which in this application was the starting point for the successful scheme outlined).

The existence of non-crystallographic symmetry implies that the crystallographic phase terms are not independent. They are coupled in a complex manner reflecting the duplicate copies of a single structure at different locations within the asymmetric unit. This joint relationship amongst the phases can be exploited to improve the experimentally determined values. In many instances, all or part of the NCS can be interpreted as arising from translationally related molecules. When this occurs, our hybrid real-space–reciprocal-space approach to phase refinement is more accurate and computationally efficient than either the exclusively real-space (Bricogne, 1974, 1976) or exclusively reciprocal-space (Rossman & Blow, 1963, 1964) approaches previously described. With our method, the averaging and unit-cell reconstruction steps are recognized to be convolutions in real space. These convolutions are more conveniently performed in reciprocal space as multiplications where the translations are incorporated analytically; hence, no interpolations are required. The imposition of a molecular boundary (necessary for phase refinement) is performed in real space as a simple multiplication instead of in reciprocal space as a convolution (Rossman & Blow, 1963, 1964), again resulting in significant time savings.

In this paper the mathematics required to perform these operations have been developed and applied to the low-resolution structure determination of α-bungarotoxin. The problem here was to transfer phases from one crystal form to another by molecular replacement methods and subsequently to refine the phases in the new unit cell (containing two copies of the molecule per as.u.). The resultant 4 Å electron density map is a significant improvement over the starting map. Since there are only two α-bungarotoxin molecules per as.u., accurate averaging and reconstruction are crucial for refinement.

For these cases where part of the non-crystallographic symmetry is translational and part is rotational about an *arbitrary* axis, interpolations must be performed with any refinement scheme. The translational component can always be dealt with as described here. The remaining rotational NCS is probably best treated in real space as described by Bricogne (1974, 1976), although it is possible to use generalized rotations (equation 10, requiring interpolations) in the reciprocal-space approach. Where applicable, however, the methods described here represent significant improvements in speed and accuracy.

This work was supported by the National Institutes of Health grant No. GM 24485 and by the National Science Foundation PCM-25407.

References

AGARD, D. A., SPENCER, S. A. & STROUD, R. M. (1981). *Proc. Natl Acad. Sci. USA*. To be submitted.

BLOOMER, A. C., CHAMPNESS, S. J., BRICOGNE, G., STADEN, R. & KLUG, A. (1978). *Nature (London)*, **276**, 362–368.

BRICOGNE, G. (1974). *Acta Cryst.* A**30**, 395–405.

BRICOGNE, G. (1976). *Acta Cryst.* A**32**, 832–847.

CHAMBERS, J. L. & STROUD, R. M. (1977). *Acta Cryst.* B**33**, 1824–1837.

CHAMBERS, J. L. & STROUD, R. M. (1979). *Acta Cryst.* B**35**, 1861–1874.

CHANG, C. C. & LEE, C. Y. (1963). *Arch. Int. Pharmacodyn. Ther.* **144**, 241–257.

CROWTHER, R. A. (1967). *Acta Cryst.* **22**, 758–764.

CROWTHER, R. A. (1969). *Acta Cryst.* B**25**, 2571–2580.

EISENBERG, D. S. (1980). Personal communication.

HARRISON, S. C., OLSON, A. J., SCHUTT, C. E., WINKLER, F. K. & BRICOGNE, G. (1978). *Nature (London)*, **276**, 368–373.

HEIDNER, E. G., FREY, T. G., HELD, J., WEISSMAN, L. J., FENNA, R. E., LEI, M., HAREL, M., KABSCH, H., SWEET, R. M. & EISENBERG, D. (1978). *J. Mol. Biol.* **122**, 163–173.

JACK, A. (1973). *Acta Cryst.* A**29**, 545–554.

LOW, B. W., PRESTON, H. S., SATO, A., ROSEN, L. S., SEARL, J. E., RUDHO, A. D. & RICHARDSON, J. S. (1976). *Proc. Natl Acad. Sci USA*, **73**, 2991–2994.

MAIN, P. & ROSSMANN, M. G. (1966). *Acta Cryst.* **21**, 67–72.

NIXON, P. E. & NORTH, A. C. T. (1976). *Acta Cryst.* A**32**, 320–332.

RICHARDS, R. M. (1968). *J. Mol. Biol.* **37**, 225–230.

ROSSMANN, M. G. & BLOW, D. M. (1963). *Acta Cryst.* **16**, 39–45.

ROSSMANN, M. G. & BLOW, D. M. (1964). *Acta Cryst.* **17**, 1474.

SIM, G. A. (1959). *Acta Cryst.* **12**, 813–815.

SPENCER, S. A. (1977). PhD Thesis. Department of Chemistry, California Institute of Technology, Pasadena, California.

STEITZ, T. A. (1980). Personal communication.

TSERNOGLOU, D. & PETSKO, G. A. (1976). *FEBS Lett.* **68**, 1–4.